Research Article | Vol. 24, No. 21 | 17 Oct 2016 | OPTICS EXPRESS 23677

Optics EXPRESS

Nanoimprinted distributed feedback lasers of solution processed hybrid perovskites

GUY L. WHITWORTH,[1] JONATHAN R. HARWELL,[1] DAVID N. MILLER,[2] GORDON J. HEDLEY,[1] WEI ZHANG,[3] HENRY J. SNAITH,[3] GRAHAM A. TURNBULL,[1,4] IFOR D. W. SAMUEL[1,5]

[1]*Organic Semiconductor Centre, SUPA, School of Physics and Astronomy, University of St Andrews, St Andrews, KY16 9SS, UK*
[2]*EastCHEM School of Chemistry, University of St. Andrews, KY16 9ST, UK*
[3]*Department of Physics, Clarendon Laboratory, University of Oxford, Oxford, OX1 3PU, UK*
[4]*gat@st-andrews.ac.uk*
[5]*idws@st-andrews.ac.uk*

Abstract: Hybrid perovskite materials have considerable potential for light emitting devices such as LEDs and lasers. We combine solution processed $CH_3NH_3PbI_3$ perovskite with UV nanoimprinted polymer gratings to fabricate distributed feedback (DFB) lasers. The lead acetate deposition route is shown to be an effective method for fabricating low-loss waveguides (loss coefficient ~6 cm-1) and highly compatible with the polymer grating substrates. The nanoimprinted perovskite exhibited single-mode band-edge lasing, confirmed by angle-dependent transmission measurements. Depending on the excitation pulse duration the lasing threshold shows a value of 110 μJ/cm2 under nanosecond pumping and 4 μJ/cm2 under femtosecond pumping. We demonstrate further that this laser has excellent stability with a lifetime of 10^8 pulses.

OCIS codes: (140.3490) Lasers, distributed-feedback; (140.3380) Laser materials.

References and links

1. M. A. Green, A. Ho-Baillie, and H. J. Snaith, "The emergence of perovskite solar cells," Nat. Photonics **8**(7), 506–514 (2014).
2. A. Kojima, K. Teshima, Y. Shirai, and T. Miyasaka, "Organometal halide perovskites as visible-light sensitizers for photovoltaic cells," J. Am. Chem. Soc. **131**(17), 6050–6051 (2009).
3. W. S. Yang, J. H. Noh, N. J. Jeon, Y. C. Kim, S. Ryu, J. Seo, and S. I. Seok, "High-performance photovoltaic perovskite layers fabricated through intramolecular exchange," Science **348**(6240), 1234–1237 (2015).
4. J. H. Noh, S. H. Im, J. H. Heo, T. N. Mandal, and S. I. Seok, "Chemical management for colorful, efficient, and stable inorganic-organic hybrid nanostructured solar cells," Nano Lett. **13**(4), 1764–1769 (2013).
5. G. Xing, N. Mathews, S. S. Lim, N. Yantara, X. Liu, D. Sabba, M. Grätzel, S. Mhaisalkar, and T. C. Sum, "Low-temperature solution-processed wavelength-tunable perovskites for lasing," Nat. Mater. **13**(5), 476–480 (2014).
6. M. Era, S. Morimoto, T. Tsutsui, and S. Saito, "Organic-inorganic heterostructure electroluminescent device using a layered perovskite semiconductor (C6H5C2H4NH3)2PbI4," Appl. Phys. Lett. **65**(6), 676–678 (1994).
7. T. Gebauer and G. Schmid, "Inorganic-organic hybrid structured LED's," Z. Anorg. Allg. Chem. **625**(7), 1124–1128 (1999).
8. H. Cho, S. H. Jeong, M. H. Park, Y. H. Kim, C. Wolf, C. L. Lee, J. H. Heo, A. Sadhanala, N. Myoung, S. Yoo, S. H. Im, R. H. Friend, and T. W. Lee, "Overcoming the electroluminescence efficiency limitations of perovskite light-emitting diodes," Science **350**(6265), 1222–1225 (2015).
9. S. Yakunin, L. Protesescu, F. Krieg, M. I. Bodnarchuk, G. Nedelcu, M. Humer, G. De Luca, M. Fiebig, W. Heiss, and M. V. Kovalenko, "Low-threshold amplified spontaneous emission and lasing from colloidal nanocrystals of caesium lead halide perovskites," Nat. Commun. **6**, 8056 (2015).
10. L. Protesescu, S. Yakunin, M. I. Bodnarchuk, F. Krieg, R. Caputo, C. H. Hendon, R. X. Yang, A. Walsh, and M. V. Kovalenko, "Nanocrystals of Cesium Lead halide perovskites (CsPbX3, X = Cl, Br, and I): Novel optoelectronic materials showing bright emission with wide color gamut," Nano Lett. **15**(6), 3692–3696 (2015).
11. H. Zhu, Y. Fu, F. Meng, X. Wu, Z. Gong, Q. Ding, M. V. Gustafsson, M. T. Trinh, S. Jin, and X.-Y. Zhu, "Lead halide perovskite nanowire lasers with low lasing thresholds and high quality factors," Nat. Mater. **14**(6), 636–642 (2015).
12. Q. Zhang, S. T. Ha, X. Liu, T. C. Sum, and Q. Xiong, "Room-temperature near-infrared high-Q perovskite

#270536 http://dx.doi.org/10.1364/OE.24.023677
Journal © 2016 Received 19 Jul 2016; revised 8 Sep 2016; accepted 20 Sep 2016; published 3 Oct 2016

Optics EXPRESS

whispering-gallery planar nanolasers," Nano Lett. **14**(10), 5995–6001 (2014).
13. B. R. Sutherland, S. Hoogland, M. M. Adachi, C. T. O. Wong, and E. H. Sargent, "Conformal organohalide perovskites enable lasing on spherical resonators," ACS Nano **8**(10), 10947–10952 (2014).
14. Q. Liao, K. Hu, H. Zhang, X. Wang, J. Yao, and H. Fu, "Perovskite microdisk microlasers self-assembled from solution," Adv. Mater. **27**(22), 3405–3410 (2015).
15. R. Dhanker, A. N. Brigeman, A. V. Larsen, R. J. Stewart, J. B. Asbury, and N. C. Giebink, "Random lasing in organo-lead halide perovskite microcrystal networks," Appl. Phys. Lett. **105**(15), 151112 (2014).
16. F. Deschler, M. Price, S. Pathak, L. E. Klintberg, D. D. Jarausch, R. Higler, S. Hüttner, T. Leijtens, S. D. Stranks, H. J. Snaith, M. Atatüre, R. T. Phillips, and R. H. Friend, "High photoluminescence efficiency and optically pumped lasing in solution-processed mixed halide perovskite semiconductors," J. Phys. Chem. Lett. **5**(8), 1421–1426 (2014).
17. S. Chen, K. Roh, J. Lee, W. K. Chong, Y. Lu, N. Mathews, T. C. Sum, and A. Nurmikko, "A photonic crystal laser from solution based organo-Lead Iodide perovskite thin films," ACS Nano **10**(4), 3959–3967 (2016).
18. Y. Jia, R. A. Kerner, A. J. Grede, A. N. Brigeman, B. P. Rand, and N. C. Giebink, "Diode-pumped organo-Lead halide perovskite lasing in a metal-clad distributed feedback resonator," Nano Lett. **16**(7), 4624–4629 (2016).
19. M. Saliba, S. M. Wood, J. B. Patel, P. K. Nayak, J. Huang, J. A. Alexander-Webber, B. Wenger, S. D. Stranks, M. T. Hörantner, J. T.-W. Wang, R. J. Nicholas, L. M. Herz, M. B. Johnston, S. M. Morris, H. J. Snaith, and M. K. Riede, "Structured organic-inorganic perovskite toward a distributed feedback laser," Adv. Mater. **28**(5), 923–929 (2016).
20. W. Zhang, S. Pathak, N. Sakai, T. Stergiopoulos, P. K. Nayak, N. K. Noel, A. A. Haghighirad, V. M. Burlakov, D. W. deQuilettes, A. Sadhanala, W. Li, L. Wang, D. S. Ginger, R. H. Friend, and H. J. Snaith, "Enhanced optoelectronic quality of perovskite thin films with hypophosphorous acid for planar heterojunction solar cells," Nat. Commun. **6**, 10030 (2015).
21. Q. Lin, A. Armin, R. C. R. Nagiri, P. L. Burn, and P. Meredith, "Electro-optics of perovskite solar cells," Nat. Photonics **9**(2), 106–112 (2014).
22. P. Löper, M. Stuckelberger, B. Niesen, J. Werner, M. Filipič, S.-J. Moon, J.-H. Yum, M. Topič, S. De Wolf, and C. Ballif, "Complex refractive index spectra of CH3NH3PbI3 perovskite thin films determined by spectroscopic ellipsometry and spectrophotometry," J. Phys. Chem. Lett. **6**(1), 66–71 (2015).
23. J. M. Ball, S. D. Stranks, M. T. Hörantner, S. Hüttner, W. Zhang, E. J. W. Crossland, I. Ramirez, M. Riede, M. B. Johnston, R. H. Friend, and H. J. Snaith, "Optical properties and limiting photocurrent of thin-film perovskite solar cells," Energy Environ. Sci. **8**(2), 602–609 (2015).
24. M. Cadelano, V. Sarritzu, N. Sestu, D. Marongiu, F. Chen, R. Piras, R. Corpino, C. M. Carbonaro, F. Quochi, M. Saba, A. Mura, and G. Bongiovanni, "Can trihalide Lead perovskites support continuous wave lasing?" Adv. Opt. Mater. **3**(11), 1557–1564 (2015).
25. J. Herrnsdorf, Y. Wang, J. J. D. Mckendry, Z. Gong, D. Massoubre, B. Guilhabert, G. Tsiminis, G. A. Turnbull, I. D. W. Samuel, N. Laurand, E. Gu, and M. D. Dawson, "Micro-LED pumped polymer laser: A discussion of future pump sources for organic lasers," Laser Photonics Rev. **7**(6), 1065–1078 (2013).
26. W. Zhang, M. Saliba, D. T. Moore, S. K. Pathak, M. T. Hörantner, T. Stergiopoulos, S. D. Stranks, G. E. Eperon, J. A. Alexander-Webber, A. Abate, A. Sadhanala, S. Yao, Y. Chen, R. H. Friend, L. A. Estroff, U. Wiesner, and H. J. Snaith, "Ultrasmooth organic-inorganic perovskite thin-film formation and crystallization for efficient planar heterojunction solar cells," Nat. Commun. **6**, 6142 (2015).
27. I. Suárez, E. J. Juárez-Pérez, J. Bisquert, I. Mora-Seró, and J. P. Martínez-Pastor, "Polymer/perovskite amplifying waveguides for active hybrid Silicon photonics," Adv. Mater. **27**(40), 6157–6162 (2015).
28. L. Qin, L. Lv, Y. Ning, C. Li, Q. Lu, L. Zhu, Y. Hu, Z. Lou, F. Teng, and Y. Hou, "Enhanced amplified spontaneous emission from morphology-controlled organic–inorganic halide perovskite films," RSC Advances **5**(125), 103674 (2015).

1. Introduction

Hybrid organic-inorganic halide perovskites have recently emerged as an important new class of optoelectronic materials [1]. Perovskite solar cells have shown by far the most rapid growth in performance of any photovoltaic technology with efficiencies now exceeding 20% [2, 3]. Most research has focused on methylammonium lead halides ($CH_3NH_3PbX_3$ where X = Cl, Br or I). By altering the halide constituent, the band-gap may be tuned from near-infrared to deep-blue [4, 5]. The $CH_3NH_3PbX_3$ thin films can be solution processed by depositing precursors onto a substrate followed by a thermal annealing process. There is now considerable interest in light-emitting devices as well as solar cells. Light-emitting diodes (LEDs) [6–8] have been demonstrated using $CH_3NH_3PbX_3$ thin films, while fully inorganic $CsPbX_3$ colloidal nanocrystals have shown photoluminescence quantum yields (PLQY) of up to 90% [9, 10].

The high brightness and band-gap tuneability has made $CH_3NH_3PbX_3$ perovskites attractive candidates as optical gain media for a new family of low-cost semiconductor lasers.

Optics EXPRESS

Combined with their high ambipolar charge mobility they have future potential to be used as visible wavelength tuneable diode lasers. Perovskite lasers have been demonstrated in several configurations: resonators including a Fabry-Perot cavity formed with parallel edge facets [11]; ring resonators in microspheres or nanoplatelets [9, 12–14]; and random lasing in scattering films [15]. These structures have supported multimode lasing spanning the full amplified spontaneous emission (ASE) bandwidth (5-10 nm). For many applications (spectroscopy, sensing, communications) laser action at user-defined wavelengths and single-mode operation is very desirable [16]. Photonic crystal single-mode perovskite lasers have recently been demonstrated using both SiO_2 and Si photonic crystals fabricated by electron beam lithography [17] and holographic lithography [18]. Here we present distributed feedback (DFB) perovskite lasers fabricated on UV nanoimprint lithography (UV-NIL) polymer gratings. This is a simple, high-throughput and fully solution processable method for DFB grating fabrication which we demonstrate to be compatible with perovskite solution processing.

To achieve high performance operation in perovskite lasers, it is important to create films with good optical performance and low scattering losses. As such, deposition methods which produce large crystallites such as thermal evaporation are less suitable for making DFB lasers [19]. Here we demonstrate DFB lasing by using the lead acetate deposition method to form a low loss optical waveguide on top of high fidelity polymer micro pillar arrays made by UV-NIL where sub-nanometre lasing spectra are observed at the band edge of the photonic dispersion. We compare laser thresholds under nano- and femto- second optical pumping and show that the perovskite lasers are very stable compared with organic semiconductor lasers, even at high repetition rates of 20 kHz, dropping to half their initial output after ~10^8 pulses.

2. $CH_3NH_3PbI_3$ solution deposited waveguides

Perovskite solutions were prepared by combining methylammonium iodide and lead acetate trihydrate, at a 3:1 molar ratio (dissolved in dimethylformamide (DMF) at 400 mg/ml). Hypophosphorous acid was also added to the solution for improved film quality and increased PLQY [20] (0.3% of the total volume) prior to deposition. Films were fabricated inside a N_2 glovebox by spin-coating solution onto substrates pre-treated by oxygen plasma ashing. DFB laser samples had an additional encapsulating layer of CYTOP spin-cast on top of the perovskite surface. Planar waveguide samples were initially fabricated by using glass substrates without encapsulation. These were used to measure the amplified spontaneous emission as well as the perovskite waveguide loss. The 450 nm output from an OPO (4 ns pulse duration, 20 Hz) (Continuum Panther) was focused to a stripe of dimensions 4 x 0.5 mm using a cylindrical lens onto a glass/perovskite film. When pumping above ASE threshold, the stimulated emission signal was collected from the edge of the film and passed through a 100 μm slit into a fibre coupled CCD spectrograph. Using a motorised stage the pump stripe was scanned across the 2.5 cm x 2.5 cm films, and the ASE signal collected at each position.

Figure 1(a) shows the measured ASE spectra centred at 788 nm and the reduction in ASE intensity detected as the stripe was moved away from the edge of the film. The reduction is due to loss in the waveguide and the decay was fitted to the equation $I_o e^{-\alpha x}$, where I_o is the initial intensity, α is the loss coefficient and x is the distance between the excitation stripe and the detection edge, giving the waveguide loss to be 6 ± 0.3 cm^{-1}.

Optics EXPRESS

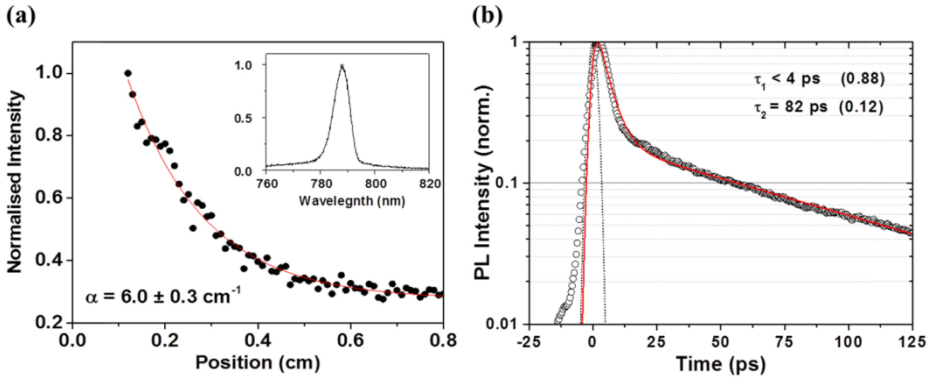

Fig. 1. (a) ASE intensity as a function of increasing distance from detection edge (black circles). The red line is a fit to an expentional decay. The inset shows the ASE spectral profile centred at 790 nm. (b) Time-resolved fluorescence data (open circles) and instrument response function (black dotted line). The red curve is the fitted decay characteristics with the exponential time constants and pre-exponential amplitudes stated.

The excited state lifetime at the ASE threshold (18 μJ/cm^2 under femtosecond pumping) was subsequently measured with a synchroscan universal streak camera (C10910) from Hamamatsu Photonics. Excitation was at 650 nm, 300 fs (FWHM) at a repetition rate of 5 kHz, which was produced as the signal output of an Orpheus OPA, pumped by a Pharos regenerative amplifier (Light Conversion). The excitation intensity was controlled with a neutral density wheel until the $CH_3NH_3PbI_3$ film was just at the ASE threshold. The time-resolved fluorescence data was then integrated over 760 nm to 820 nm to plot the excited state dynamics of the perovskite films, [Fig. 1(b)] displaying an initial instrument response limited decay followed by a longer 82 ps tail.

3. Nano-imprinted $CH_3NH_3PbI_3$ laser fabrication

Distributed feedback cavities are formed via the high reflectivity of a periodic nanostructure near the photonic band edge, and can be achieved by simple deposition of a gain medium onto a pre-structured surface. Lasing occurs when the Bragg condition, $2n_{eff}\Lambda = m\lambda_b$ is met, where n_{eff} is the effective refractive index, Λ is the grating period, m is the diffractive order and λ_b is the feedback wavelength. Using an EVG 620 photomask aligner with custom NIL tooling a perfluoro-polyether daughter stamp was cast from a silicon master structure (cured by UV exposure) and subsequently used to nanoimprint into a spin-coated UVCur06 film under UV exposure. To fabricate the DFB lasers the perovskite precursor was then spin-coated onto UV Cur06 nanoimprinted gratings fabricated by UV-NIL. A schematic cross-section of the perovskite DFB laser is shown in Fig. 2(a). The fluorinated polymer CYTOP was used as a hydrophobic encapsulant to prevent moisture from degrading the samples.

Nanoimprinted perovskite structures (without CYTOP encapsulant) were imaged in a dual-beam scanning electron microscope (SEM)/focussed ion-beam (FIB) system. A layer of gold (1-10 nm) was sputtered on top of $CH_3NH_3PbI_3$/UVCur06 samples using a Quorum Q150R ES stutterer to avoid any charging effects. Samples were then placed into an FEI Scios^{TM} DualBeam system for carbon deposition, FIB etching and SEM imaging. Figure 2(b) shows an inclined SEM image (52°) of the surface of a perovskite film over the top of the grating. A portion of the perovskite has been removed to reveal the 2D pillar array underneath achieved by using the FIB in imaging mode with a flux strong enough to strip away the perovskite layer whilst leaving the more resilient UVCur06 layer unaffected. The perovskite film planarises the grating, with only its intrinsic surface roughness apparent on the top

Optics EXPRESS

surface. Images were also taken of the perovskite surface over unstructured regions for comparison [Fig. 2(c)]. Crystal domains were observed with lateral size ~300 ± 100 nm.

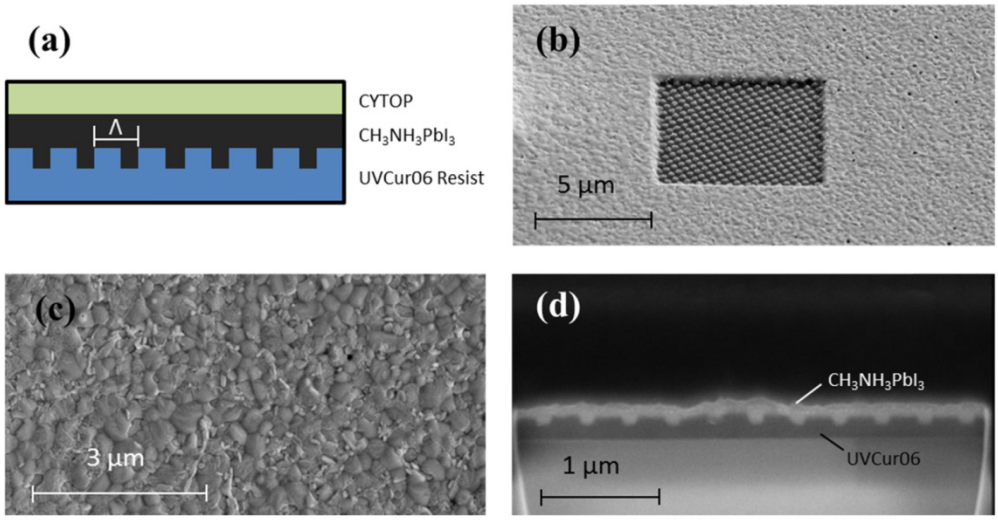

Fig. 2. SEM images of neat $CH_3NH_3PbI_3$ and DFB samples. (a) Schematic of $CH_3NH_3PbI_3$ DFB laser with encapsulating CYTOP layer. (b) SEM image at a 52° inclination to the normal of $CH_3NH_3PbI_3$ on top of the grating with a portion of the perovskite removed by FIB. (c) SEM image of the surface of $CH_3NH_3PbI_3$ on a planar substrate. (d) Cross-sectional SEM image of a FIB etched trench showing the perovskite layer on top of the UV nanoimprinted grating. The sample area has a carbon layer deposited on top of the $CH_3NH_3PbI_3$ for good image contrast (upper black layer). The grating in the perovskite layer can be clearly seen at the interface with the nanoimprinted layer (UVCur06).

The FIB was used to mill directly through the perovskite laser to image the cross-section of the DFB grating [Fig. 2(d)]. Prior to milling, a carbon layer (black upper layer) was electro-deposited onto the surface of the $CH_3NH_3PbI_3$ film. This acted as a protective layer to provide a clean vertical cut as well as a layer to provide a high contrast with the perovskite. The grating period can be measured from this cross-section to be Λ = 365 nm with a 2D fill factor of 0.6 and a grating height of ~80 nm. The perovskite layer sits an extra ~145 nm above the grating peaks.

4. $CH_3NH_3PbI_3$ distributed feedback lasing

Perovskite DFB lasers were optically pumped using both nanosecond and femtosecond laser sources. Nanosecond 355 nm excitation pulses were generated by a diode-pumped solid-state (DPSS) passively Q-switched laser source (FTSS355-Q2-OEM, CryLas GmbH) at 100 Hz and pulse duration of 0.91 ns. Spectral emission was collected by a fibre coupled Andor CCD spectrometer, collecting light at normal incidence to the samples. Laser pulses were focused to a spot diameter of 0.5 mm on the perovskite DFB samples to generate laser action. All spectroscopy measurements were carried out in air.

A clear line narrowing was observed in the emission spectra [Figs. 3(b)-3(e)], above a threshold of pulse density of 110 µJ/cm^2, centred at 784 nm. This line narrowing was accompanied by a super-linear increase in the optical output [Fig. 3(a)]. At 120 µJ/cm^2 pump fluence, the emission spectrum collapsed to a narrow < 0.4 nm full-width-at-half-maximum (FWHM) lasing peak. This peak broadened slightly at higher pumping intensity to ~0.6 nm where some multimodal behaviour became evident in the spectrum. Using the Bragg equation, the lasing wavelength implies an effective index of n_{eff} = 2.15, assuming second order diffraction.

Optics EXPRESS

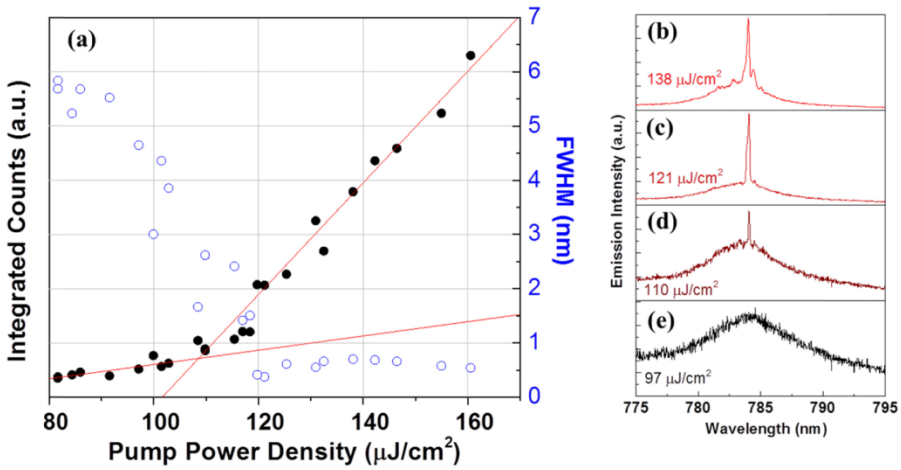

Fig. 3. Distributed feedback lasing spectra from structured $CH_3NH_3PbI_3$ films. (a) Input/output power characteristic with linear fits plotted for low and high energy data points (black), along with corresponding FWHM (blue). (b-e) Following a 355 nm nanosecond pulsed excitation, emission spectra from the DFB sample shown with corresponding pump energy density.

To confirm that the observed lasing arises from the DFB structure, angle dependent transmission measurements were made using a J.A. Woollham spectroscopic ellipsometer. When the beam was directed through the grating area, a distinctive coupling dip was observed in the transmission spectrum. Figure 4(a) shows the angle dependent transmission of the DFB samples. This image shows an optical resonance, the wavelength of which varies with the light beam angle of incidence, showing the coupling of the periodic grating to a waveguide mode. The spectral position of the crossing of this resonance at normal incidence ($\theta = 0°$) is λ_b for distributed feedback structures. From Fig. 4(a) we determine $\lambda_b = 783$ nm, close to the DFB laser wavelength of 784 nm. We note that the ellipsometer used for Fig. 4(a) has a resolution of ~1.5 nm which is not high enough to directly measure the photonic stop band itself.

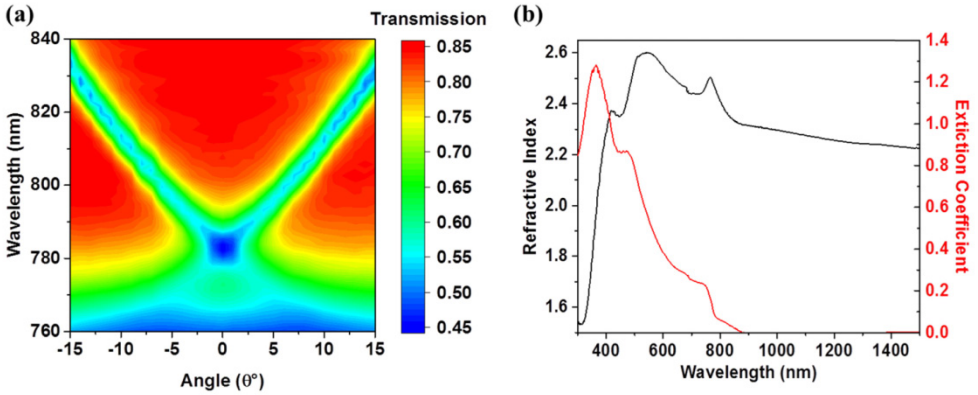

Fig. 4. Photonic dispersion in $CH_3NH_3PbI_3$. (a) Angle dependent transmission spectra normalised by the planar film transmission. (b) Refractive indices and extinction coefficients of $CH_3NH_3PbI_3$ measured using spectroscopic ellipsometry.

The ellipsometer was also used to determine the refractive index of the perovskite films. A wide range of refractive indices has previously been reported in the literature, ranging from 2.4 – 2.8 in the emission region [21–23]. The refractive index measured here at 783 nm was found to be, $n_{783} = 2.458$, agreeing closely with *Löper* et al [22]. The thickness of the planar

Optics EXPRESS

films of $CH_3NH_3PbI_3$ was measured to be ~190 nm by surface profilometry. Taking the refractive index of the UVCur06 layer (measured by ellipsometry) and the cladding layer CYTOP to be 1.535 and 1.335 respectively the effective refractive index of the waveguide was calculated to be n_{eff} = 2.14. This is in excellent agreement with the value n_{eff} = 2.15 obtained from the Bragg equation. The 0.5% difference in these values is accounted for by the uncertainty in the refractive index data and thickness measurements.

The effect of pump laser pulse duration was investigated by replacing the nanosecond laser source with a femtosecond laser (pulse duration ~200 fs). Femtosecond pulses were generated by the 515 nm 2nd harmonic of a PHAROS regenerative amplifier, with 200 fs pulses, with the repetition rate reduced from 100 kHz to 20k Hz using a pulse picker. A fibred coupled OceanOptics USB spectrometer in the femtosecond pumping experiments. With the pump pulse shorter than the electron-hole recombination lifetime of the perovskite we observe a substantial reduction in lasing threshold, by almost two orders of magnitude to 4 μJ/cm^2 [Fig. 5(a)]. Under femtosecond excitation it was seen that the lasers exhibited much higher stability than is typical for an organic laser in air. For pumping at 20 kHz (7 μJ/cm^2) in air, the $CH_3NH_3PbI_3$ laser output decreased to half its initial maximum after 10^8 pulses as shown in Fig. 5(b). The stability at high repetition rates indicates that perovskites may be able to sustain continuous wave operation [17, 18, 24].

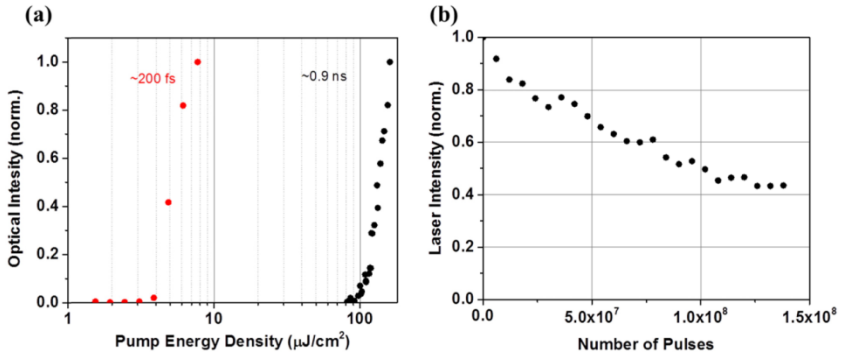

Fig. 5. Femtosecond and nanosecond optical pumping of $CH_3NH_3PbI_3$ DFB lasers. (a) Input/output threshold characteristic of femtosecond (red) and nanosecond (black) optical pumping. Nanosecond data the same as shown in Fig. 3(a). (b) Lasing stability data of $CH_3NH_3PbI_3$ DFB laser under femtosecond pumping operating at 20 kHz.

5. Discussion

The much higher threshold for nanosecond pumping can largely be attributed to the pulses being much longer than the fluorescence lifetime [25] [Fig. 1(a)]. We can compare the lasing thresholds more accurately by considering the excitation density threshold for lasing over the course of the lifetime of the excited states (82 ps). This yields excitation density thresholds of ρ_{ns} = 9.1 x10^{23} cm^{-3} and of ρ_{fs} = 5.1 x10^{23} cm^{-3} for nanosecond and femtosecond pumping respectively, bring them in much closer agreement with each other.

A key factor to achieve single mode DFB lasing is to fabricate a high quality periodic waveguide [Fig. 2(a)]. Filling the grating grooves and having a smooth perovskite surface minimises waveguide losses, lowering the DFB lasing threshold. This was achieved by choosing the lead acetate precursor route for the fabrication of $CH_3NH_3PbI_3$ films by spin-coating. This method has been shown to give much smoother films than other deposition methods such as evaporated crystals [26], creating relatively low loss waveguides with loss coefficient, $\alpha = 6 \pm 0.3$ cm^{-1} [Fig. 1(a)], much smaller than some previously reported perovskite waveguide losses (19-21 cm^{-1}) [27] comparable with others for $CH_3NH_3PbI_3$ perovskite films deposited from DMF (6.7 cm^{-1}) [28]. In comparison to more established DFB lasers, these perovskite films still have very high surface roughness as shown in Fig.

Optics EXPRESS

2(b)-2(d). If smoother films could be fabricated with improved deposition methods we would expect the lasing threshold to be lowered, increasing the future applicability of perovskite lasers. The negative effect of the surface roughness can be seen in Fig. 3(b); at high pump intensities random lasing modes can be seen to emerge in the background of the DFB laser spectrum.

6. Conclusion

In conclusion, we have demonstrated simple fabrication of a solution-processed $CH_3NH_3PbI_3$ distributed feedback laser using nanoimprinted polymer gratings. The laser shows single frequency lasing at the stop band edge of the photonic structure. SEM images of the perovskite surface and a cross-sectional image of the waveguide demonstrate that the solution processed $CH_3NH_3PbI_3$ formed via the lead acetate route can fill sub-micron structures well and that the surface is unperturbed by the presence of the grating underneath. Under femtosecond excitation the perovskite laser exhibits a low lasing threshold of 4 $\mu J/cm^2$ and high stability with a half-life of 10^8 pulses. These results show that perovskite materials provide a promising new route to low-cost fully solution-processed lasers.

Funding

This work was supported by the Engineering and Physical Sciences Research Council (EPSRC) of the UK Grants; EP/K503162/1, EP/M506631/1, EP/M025330/1 and EP/L017008/1. IDWS acknowledges funding from a Royal Society Wolfson research merit award.

Data and materials availability

All presented data can be found at DOI: 10.17630/126aaf5b-3a8e-464c-beb0-0ec6724ab582.